Article

JOURNAL OF COMPOSITE MATERIALS

Journal of Composite Materials
2015, Vol. 49(11) 1393–1406

DOI: 10.1177/0021998314534705
jcm.sagepub.com
SAGE

Oxidation-induced damage evolution in a unidirectional polymer matrix composite

Jianyong Liang and Kishore V Pochiraju

Abstract

Long-term degradation and failure in high-temperature polymer matrix composites are driven by chemical changes due to oxidation reactions and damage evolution. In this paper, we present a methodology for simulating oxidation-induced damage in a unidirectional composite. This approach explicitly models the time-dependent growth of oxidation layers and the evolution of discrete cracking in a homogenized representation of the composite. Long-term isothermal aging is simulated with high-resolution tracking of morphological changes and damage evolution. An element-free Galerkin method is used to simulate the oxidation layer growth, and the extended finite element method is used for computing the stress fields and predicting damage. The developed model captures both oxidation and damage growth in the unidirectional lamina through long periods of oxidative aging. The model predictions correlate well with the experimental results for a carbon/polyimide composite system.

Keywords

Oxidation growth, damage evolution, extended finite element method, oxidation-mechanics-damage model, failure mode

Introduction

Polymer composites with durability in high-temperature environments (100–350°C) are desired for lightweight aerospace structures and propulsion system applications. However, the durability of the high-temperature polymer matrix composites (HTPMCs) tends to be limited due to environmental degradation. The age-related degradation in HTPMCs is the physical change due to creep and relaxation of the constituent materials, chemical changes due to long-term polymerization and oxidation reactions, weakening of chemically changing materials and volumetric strains induced by chemical changes, and damage driven by applied loading. In this paper, we focus on the damage evolution in composites due to oxidation under long-term (thousands of hours) use under high-temperature isothermal conditions.

The morphological changes during aging in oxidative environments are due to oxygen adsorption, diffusion into the interior, and reaction with the constituent materials.[1] While both carbon and glass fibers may be stable at operating temperatures under 300°C, the dissolved oxygen reacts with the polymer matrix and degrades the composite. The effect of oxidation reactions on the morphology of the composite material has been tracked in an earlier effort by defining an oxidation-state variable (ϕ).[2] A mismatch strain accompanies the chemical changes, with the outer oxidized layers shrinking with respect to the unoxidized interior.[3] The strain induced by the oxidation and weak-oxidized layers leads to matrix cracking and interface debonding.[4] Discrete cracks open up new surfaces and allow oxygen to diffuse deeper into the material.[2,5] The high-strain state in the vicinity of cracks accelerates oxygen diffusivity in the material.[5] Therefore, oxidation and damage growth form a strongly coupled degradation cycle with each accelerating the other.[6]

Oxidation in polymers has been extensively studied in the last decade. Colin et al.[7] used a mechanistic model for oxidation reactions, and others have used weight loss to track the bulk thermo-oxidative stability of the materials.[8–10] Pochiraju and Tandon[2]

Department of Mechanical Engineering, Stevens Institute of Technology, Hoboken, NJ, USA

Corresponding author:
Kishore V Pochiraju, Department of Mechanical Engineering, Stevens Institute of Technology, C-301 Castle Point on Hudson, Hoboken, NJ 07030, USA.
Email: kishore.pochiraju@stevens.edu

investigated the oxidation-induced chemical changes in the materials using an oxidation-state variable (Ø) that defines a measure of oxidation extent at any material point in the structure. In this model, the material transitions irreversibly from unoxidized or pristine ($Ø_{un}$) and completely oxidized ($Ø_{ox}$) states. Oxidation-state-dependent constitutive relationships for thermal, diffusive, and mechanical behaviors of the materials are formulated to predict the material performance during oxidation. The oxidation-induced shrinkage[3] and oxidation growth with an assumed crack propagation rate[6] have been investigated earlier. In this paper, we present a coupled oxidation-damage growth model that simulates damage evolution in unidirectional composite lamina during isothermal aging. This developed model easily lends itself to the analysis of laminated composites. Damage initiation and crack growth are simulated from oxidation-state-dependent failure criteria. No assumptions were made regarding the crack location, propagation direction, or rate of growth.

Finite element methods have been extensively used to simulate damage growth but with defined initial damage states and/or propagation paths.[11,12] Modeling arbitrary crack paths requires re-meshing for incorporating new cracking boundaries,[13] conforming to geometric discontinuities, and refining solutions near the crack tip. Modeling a growing crack with re-meshing is particularly cumbersome for oxidation problems because the mesh must be updated continuously to match the geometry of the crack and morphological changes due to oxidation. In this effort, we use a multi-mesh method in which element-free Galerkin simulation determines the morphological changes, and the extended finite element method (XFEM) tracks stress and damage.[14,15] The two simulations run concurrently, and the close coupling between oxidation and damage growth is incorporated into the model with frequent updates of oxidation and damage states.

Coupled oxidation growth and damage evolution

A schematic of the mechanisms driving the oxidation-induced damage is shown in Figure 1. The figure depicts a [0/90] laminate exposed on one edge to an oxidizing environment. As the structure ages in the oxidative environment, an oxidized zone develops and grows from the exposed surface into the interior. Oxidation growth is dependent on orthotropy in the material behavior and is expected to be faster along the fiber due to higher oxygen diffusivity in that direction.[16] Oxidation in the material is accompanied by volume changes, and the resulting mismatch strain initiates discrete cracks in the material. Furthermore, the cracked surfaces adsorb oxygen, and the oxidation in

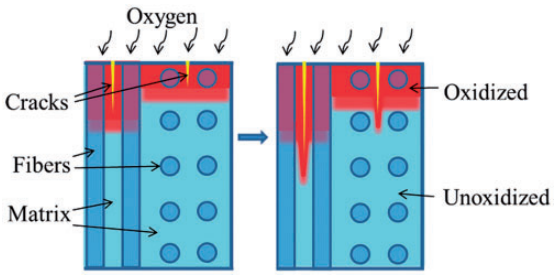

Figure 1. Schematic representation of oxidation and crack growth in a composite lamina.

the vicinity of cracks is heterogeneous while oxidized layer thickness in regions free from damage tends to be uniform.[4]

In order to capture both the anisotropy and heterogeneity of the oxidation growth and damage evolution, a multi-domain framework has been formulated. The framework divides the problem into three cooperative simulations, which are executed concurrently. Figure 2 shows a schematic of the three models and the data flow between them. As oxidation takes place over thousands of hours, the time increment at which the simulations are executed is set at 1–200 h. The time increment can be reduced, with additional computational burden, to increase the spatial resolution of the prediction. Changes in the morphology of the composites are determined over the time increment using an oxidation model, and a snapshot of the oxidation state (Ø) is determined. The stiffness, strength, and toughness at each material point are then updated with appropriate constitutive relationships, and a mechanics model determines the stress state. A damage model then evaluates the damage state (φ) using crack initiation and evolution criteria and communicates it to the oxidation and mechanics models. The cracked boundaries are updated in the oxidation model with appropriate sorption boundary conditions, and the oxidation simulation is carried out at the end of the next time increment.

Figure 3 shows the execution sequence and parameter flow of oxidation-mechanics-damage models. A time increment of a hundred hours is assumed, and morphological changes due to oxidation are computed at the end of the time increment. The oxidation model solves the oxygen diffusion-reaction kinetics with a time step of 100 h. The oxidation-state field is computed at the end of the selected time increment. The oxidation state is communicated to the mechanics model, which estimates the mechanical properties of the material and appropriate increments to the oxidation-induced strain field. The deformation and stress fields are then computed by solving the appropriate equilibrium equations, and a damage analysis is performed. The damage analysis uses a failure criterion to identify the locations of crack initiation and the direction of propagation.

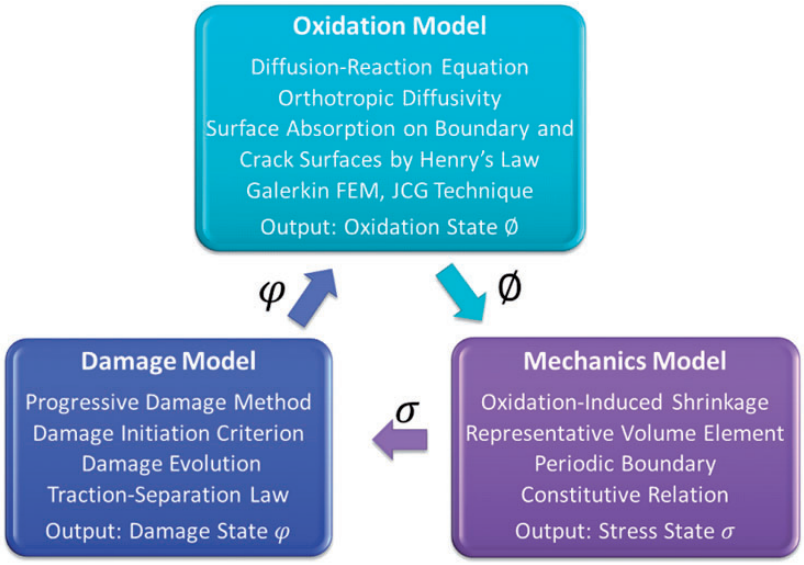

Figure 2. The oxidation-mechanics-damage model and parameter flow.

A toughness-based cohesive law determines the extent of cracking. A geometric analysis is then performed to delineate cracks that have sorption conditions and internal cracks without oxidation conditions. The oxidation model is updated with oxygen-adsorption conditions on the newly formed crack surfaces that are connected to boundaries already exposed to oxygen.

Homogenized representative volume element (RVE) with orthotropic material behavior has been used in this analysis. Figure 4 shows the schematic representation of a unidirectional composite, and the two RVEs are chosen for oxidation analysis in axial and transverse directions, respectively. The figure shows the reference coordinate system with fiber axis (L-direction) and the transverse directions (T- and Z-directions). The sizes of the RVEs differed as both the expected extent of oxidation and crack penetration varies based on the fiber orientation. Both RVEs have one boundary face exposed to the environment and the other five faces (interior faces) created by periodicity. The exposed faces have oxygen-sorption boundary condition in the diffusion-reaction equation (oxidation model), and interior faces have zero-flux condition.

Oxidation model

The oxidation model[2] computes an oxidation-state field $\phi(x,y,z;t)$ using physics-based simulation of oxygen diffusion into the composite and reactions with its constituents. Material points with pristine or unoxidized material at any time assign an oxidation-state value of $\phi(x,y,z;t)=\phi_{un}$, and completely oxidized material assigns $\phi(x,y,z;t)=\phi_{ox}$ with $\phi_{un}>\phi_{ox.}$ Material is actively oxidizing in regions where $\emptyset_{ox}<\emptyset<\emptyset_{un}$. Oxidation originates from the exposed faces and moves deeper into the material with time. Typically, $\emptyset_{un}$ is taken as unity while $\emptyset_{ox}$ assigns a finite value depending upon the residual weight of the completely oxidized constitutive material. The transition from $\emptyset_{un}=1$ to $\emptyset_{ox}$ (<1) during oxidation can be correlated with weight loss observations.[2,17]

At the temperature under consideration (177–343°C), carbon fiber is relatively stable against oxidative reactions,[18] but higher oxygen diffusivity along fiber direction contributes to faster oxidation layer growth in axial direction (L) of the lamina.[16] Also, the interphase region between fiber and matrix may be diffusive and contributes to an increased oxidation layer growth rates.[3,16] Any fiber-matrix debonding or transverse cracks provide additional pathways for oxygen to diffuse into the interior of the material.[2,8,19] Anisotropy was observed for unidirectional composites, and oxidation and damage growth rates are much higher in axial direction than that in the transverse direction.

The oxidation reaction is controlled by the oxygen concentration in the material, especially when the dissolved oxygen concentration is much lower than the saturation concentration on oxygen sorption boundary.[9] The dissolved oxygen concentration in the solid (molar volume), $C(x,y,z;t,T;V_f)$, in the homogenized composite material is a spatially and temporally varying field that depends upon the temperature (T) and fiber volume fraction (V_f). We assume that both diffusion and reaction are strain independent in this analysis. The diffusion-reaction model (governing equation)

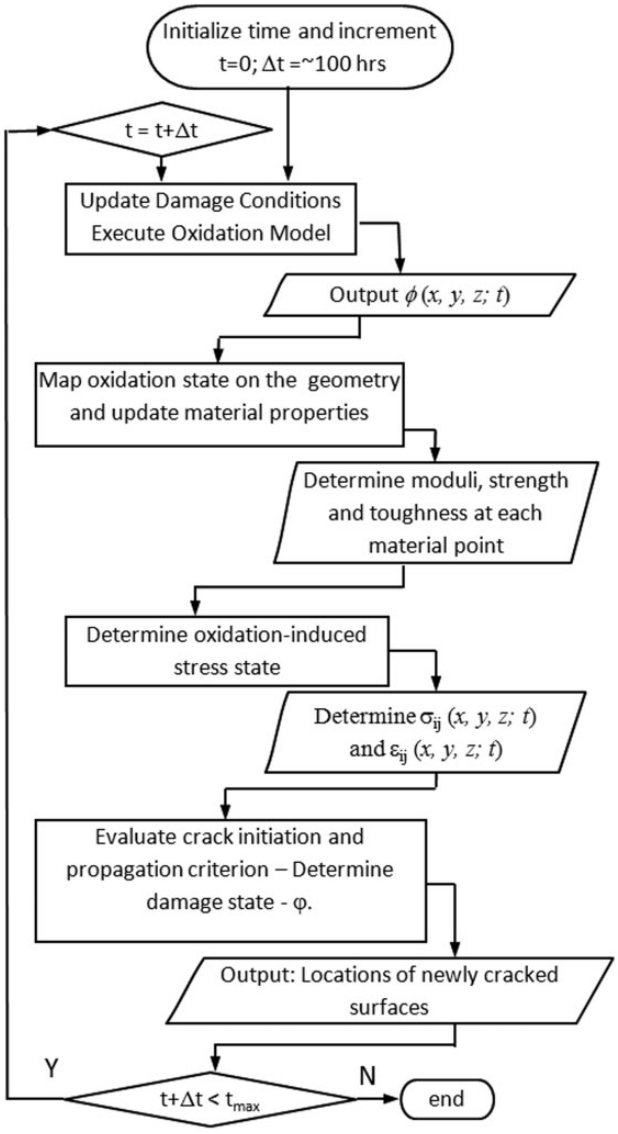

Figure 3. Flowchart for the coupled multi-domain oxidation-mechanics-damage modeling.

with orthotropic diffusivity for homogenized material is given by equation (1).

$$\frac{\partial C}{\partial t} = \left(D_L \frac{\partial^2 C}{\partial x^2} + D_T \frac{\partial^2 C}{\partial y^2} + D_Z \frac{\partial^2 C}{\partial z^2} \right) - R(\emptyset, T, C, V_f) \tag{1}$$

D_L is oxygen diffusivity along longitudinal direction and D_T and D_Z along transverse directions (T and Z directions, respectively). The effective oxygen diffusivity of the homogenized composites is interpolated based on the oxidation state as follows

$$D_{L,T,Z}(\emptyset, T, V_f) = \left[D^{un}_{L,T,Z}(T, V_f) \left(\frac{\emptyset - \emptyset_{ox}}{\emptyset_{un} - \emptyset_{ox}} \right) + D^{ox}_{L,T,Z}(T, V_f) \left(\frac{\emptyset_{un} - \emptyset}{\emptyset_{un} - \emptyset_{ox}} \right) \right] \tag{2}$$

The oxidation reaction rate of polymers is dependent on temperature,[10] oxygen concentration (which is controlled by oxygen diffusion), and the oxidation state of the material.[2] The fiber is considered non-reactive but diffusive at this temperature.[20] The oxidation reaction rate for the homogenized composite with only the resin undergoing oxidation reactions can be written as follows

$$R(\emptyset, T, C, V_f) = R_0 \frac{2\beta C}{1 + \beta C} \left[1 - \frac{\beta C}{2(1 + \beta C)} \right] \times \left(\frac{\emptyset - \emptyset_{ox}}{\emptyset_{un} - \emptyset_{ox}} \right) (1 - V_f) \tag{3}$$

The constant β controls the reaction-rate dependence on the molar concentration.[2] Temperature dependence of the saturation reaction rate is assumed in Arrhenius form as given by equation (4). Since isothermal aging is considered and the saturation reaction rate R_0 is determined at operating temperatures, the consequences of

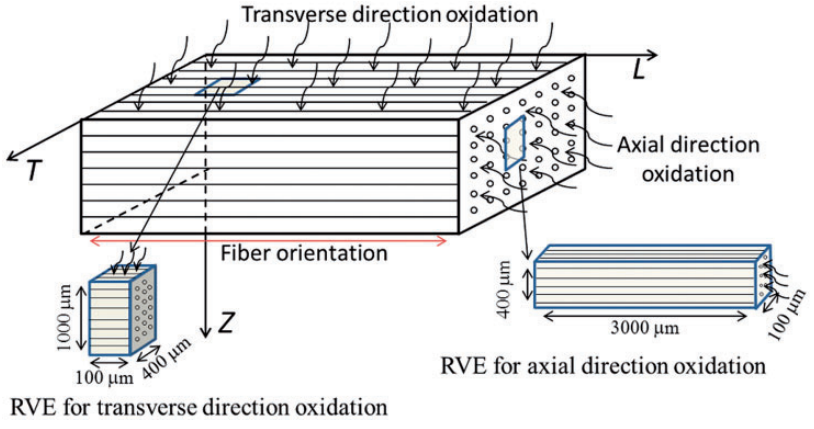

Figure 4. Geometry, reference coordinate systems, and RVE used in the analysis. RVE: representative volume element.

the Arrhenius assumption on the predictions described in this paper are minimal

$$R_0 = R_0^* exp\left(-R_a/RT\right) \tag{4}$$

In equation (4), R_0^* and R_a are the scaling and activation constants.

The oxidation-state variable $\emptyset$ indicates the availability of an active polymer site for reaction. When $\emptyset$ reaches the cut-off value $\emptyset_{\text{ox}}$, the polymer resin is assumed to be completely oxidized, and the oxygen is assumed to predominantly diffuse in the oxidized polymer rather than react with the polymer. Therefore, the oxidation-state variable $\emptyset$ tracks the conversion of the polymer into completely oxidized state. The oxidation state is related with the reaction rate $R\left(\emptyset, T, C, V_f\right)$ and aging time t as follows

$$\emptyset = max\left\{\emptyset_{ox}, \left(1 - \int_0^t \alpha(\zeta) R(\zeta) \mathrm{d}\zeta\right)\right\} \tag{5}$$

The boundaries of the material exposed to oxygen are subjected to Dirichlet conditions from Henry's law. A saturation concentration, $\mathrm{C_s} = \mathrm{SP}$, where S is the solubility and P is the partial pressure of the diffusing gas, is prescribed on the exposed boundaries. The periodic boundaries (on interior faces) or unexposed surfaces are subjected to flux-free conditions. Equation (1) is solved over a three-dimensional domain subjected to the boundary conditions using an element-free Galerkin method, which has been described in detail in earlier papers.[2,3]

Mechanics model

High-temperature aging in oxidative environments causes both physical shrinkage (dependent on time t) and chemical shrinkage (dependent on both time t and oxidation state $\emptyset$) in the resin. Due to the mismatch of oxidation-induced strain between oxidized and unoxidized materials, substantial amount of localized micromechanical stress is generated.[3,21] The oxidation-induced stress drives damage initiation and crack growth. The effective shrinkage coefficients are determined by volume averaging the fiber, unoxidized matrix, and oxidized matrix-shrinkage coefficients using energy principles,[22] and the homogenized shrinkage coefficients for both oxidized and unoxidized composite lamina can be obtained. Note that these are isothermal-shrinkage coefficients, and aging temperature has substantial influence on the shrinkage values.

The homogenized shrinkage coefficients for the unoxidized composite in axial (L-direction) and transverse directions (T- and Z-directions) can be obtained from physical shrinkage coefficients of the resin (α_m^{un}) as follows

$$\alpha_L^{un} = \left(\alpha_f E_f V_f + \alpha_m^{un} E_m^{un} V_m\right) / E_L^{un} \tag{6}$$

$$\alpha_{T,Z}^{un} = \left(1 + v_f\right)\alpha_f V_f + (1 + v_m)\alpha_m^{un} V_m - \alpha_L^{un} v_{LT} \tag{7}$$

where α_m^{un} is the shrinkage coefficient of unoxidized resin and v_m is the Poisson's ratio for the resin, which is assumed constant during oxidation. V_f and V_m are the fiber and matrix volume fractions, respectively. E_m^{un} is the elastic modulus of unoxidized resin and E_L^{un} is the homogenized elastic modulus of unoxidized composite. $\alpha_f = 0$ as fiber keep stable during thermal aging.

The homogenized material-shrinkage coefficients for completely oxidized composite lamina in axial and transverse directions are given by

$$\alpha_L^{ox} = \left(\alpha_f E_f V_f + \alpha_m^{ox} E_m^{ox} V_m\right) / E_L^{ox} \tag{8}$$

$$\alpha_{T,Z}^{ox} = \left(1 + v_f\right)\alpha_f V_f + (1 + v_m)\alpha_m^{ox} V_m - \alpha_L^{ox} v_{LT} \tag{9}$$

where α_m^{ox} is the shrinkage coefficient for oxidized resin, E_m^{ox} is the elastic modulus of oxidized resin, and E_L^{ox} is the homogenized elastic modulus of oxidized composite, which is obtained using rule-of-mixture.

For an initially mechanically stress-free structure, the oxidation-induced shrinkage strain (physical and chemical strain) during oxidative aging is divided into a time-dependent and oxidation-state-dependent component. At any material point in the structure, the shrinkage strain $\varepsilon_{L,T,Z}(\emptyset, t)$ for the composite with an arbitrary oxidation state ($\emptyset$) and aging for t hours is linearly interpolated based on the oxidation state as follows

$$\varepsilon_{L,T,Z}(\emptyset, t) = \left[\alpha_{L,T,Z}^{un}\left(\frac{\emptyset - \emptyset_{ox}}{\emptyset_{un} - \emptyset_{ox}}\right) + \alpha_{L,T,Z}^{ox}\left(\frac{\emptyset_{un} - \emptyset}{\emptyset_{un} - \emptyset_{ox}}\right)\right] \times t \tag{10}$$

The deformation and stress fields in the structure due to oxidation are then computed everywhere in the structure by solving the governing equilibrium equations and appropriate boundary conditions with XFEM.[14,23] The interpolation functions are enriched in XFEM, with additional degrees of freedom in the selected nodes around the discontinuity to describe the location of this discontinuity (crack). The approximation for a displacement vector function u with the enrichment is as follows

$$u(\bar{x}) = \sum_{I=1}^{N} N_I(\bar{x}) u_I + \sum_{J=1}^{N^f} N_J(\bar{x}) H(\bar{x}) a_J \tag{11}$$

where $N_I(\bar{x})$ is the usual nodal shape function and $H(\bar{x})$ the enrichment function (level-set functions). N is the number of finite element mesh nodes and N^f the number of enriched nodes of the mesh. u_I is the usual nodal-displacement vector associated with the continuous part of the finite element solution and a_J the additional enriched degrees of freedom at the Jth node.

Damage model

Matrix cracking and interphase debonding are commonly observed in unidirectional composite lamina.[24–27] In this effort, we use the Hashin's failure criterion[28,29] to identify locations of crack initiation and the modes of failure. The lamina failure criteria were tracked based on axial failure criterion under tension as given by equation (12), transverse failure under tension as given by equation (13), and the transverse compressive failure as given by equation (14).

Tensile/axial failure mode

$$\left(\frac{\sigma_L}{F_L^t}\right)^2+\frac{\left(\sigma_{LT}^2+\sigma_{LZ}^2\right)}{\left(F_{LT}^s\right)^2}=1 \tag{12}$$

Tensile/transverse failure mode

$$\left(\frac{\sigma_T+\sigma_Z}{F_T^t}\right)^2+\frac{\left(\sigma_{TZ}^2-\sigma_T\sigma_Z\right)}{\left(F_{TZ}^s\right)^2}+\left(\frac{\sigma_{LT}}{F_{LT}^s}\right)^2+\left(\frac{\sigma_{ZL}}{F_{LZ}^s}\right)^2=1 \tag{13}$$

Compression/transverse failure mode

$$\left[\left(\frac{\sigma_T}{2F_{TZ}^s}\right)^2-1\right]\frac{(\sigma_T+\sigma_Z)}{F_T^c}+\left(\frac{\sigma_T+\sigma_Z}{2F_{TZ}^s}\right)^2+\frac{\left(\sigma_{TZ}^2-\sigma_T\sigma_Z\right)}{\left(F_{TZ}^s\right)^2}+\left(\frac{\sigma_{LT}}{F_{LT}^s}\right)^2+\left(\frac{\sigma_{LZ}}{F_{LZ}^s}\right)^2=1 \tag{14}$$

For the stress components in above equations, σ_L, σ_T, and σ_Z represent the normal stress in L, T, and Z-direction, respectively, while σ_{LT}, σ_{LZ}, and σ_{TZ} represent the shear stress in L–T, L–Z, and T–Z planes, respectively. The strengths of the composite lamina are given by $F_i^{t,c,s}$, with the superscripts denoting tension, compression, and shear strength, respectively, and the subscripts denoting the direction of the normal strength and plane of the shear strength. It should be noted here that F_L^t is not the traditional failure strength of lamina in fiber direction, which is controlled by the fiber strength and can be obtained using law of mixture. During thermal aging of composite lamina, matrix cracking and fiber bridging occur, and the cracks propagate in the matrix around the fibers, rather than breaking the fibers. The matrix strength and fracture toughness are greatly reinforced by fiber bridging. F_L^t is defined here as the oxidative failure strength of composite lamina in L-direction (axial direction).

The mechanical properties of composites are subject to variability due to heterogeneity in microstructure.[30] Fiber spacing, void distribution, and porosity due to oxidation are natural causes of strength variability in the lamina.[31] Therefore, we spatially vary the strength of composite material by randomly assigning the strength from a probability density function.[30,32,33] We assume that the variability in strength can be modeled by a normal distribution characterized by a defined mean and variance.[34] At every material point, the strength values are sampled from the normally distributed probability distribution. The unoxidized material is considered to have a low variability, and the oxidized material is assigned substantially larger variance. Another reason for considering variability to the strength value is to localize and initiate discrete cracking in the model at a weakest point. The strength variability distribution model and the parameter used for the oxidized regions were neither observed from experiments nor characterized from the published data. We need the assumption on the strength variability to determine discrete locations in the model where damage initiates when large regions of the model are under the same stress state. Experimental characterization of strength and toughness of oxidized regions and their variability is a cumbersome and challenging proposition for an arbitrary composite system.

We determine the crack-propagation path for each failure mode based on the principal plane corresponding to the maximum principal stress in the material point. In axial-direction oxidation problem, the failure is predominately along fiber direction, and only the tensile/transverse failure mode (equation (13)) was reached during analysis. So, a constraint is placed that the crack propagates along the L-direction (axial direction) only to reduce the computation burden. In transverse oxidation, the crack menders in the oxidized region based on normal and shear stress tensor. No constraints were placed on the crack propagation path for the transverse analysis, and the direction is controlled by the maximum principal stress in the T–Z plane.

In this analysis, XFEM methods are used with level-set function to determine the crack-surface location. Material ahead of a crack tip is modeled using cohesive elements and a traction-separation law that controls the creation of new crack surfaces during damage evolution. An initially linear-elastic behavior is assumed for the traction-separation model, followed by the initiation and evolution of damage.[33] After the damage initiation criterion is met, the damage evolution starts

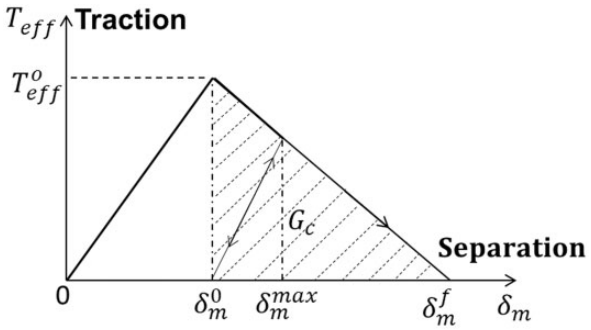

Figure 5. Traction-separation law for the cohesive damage growth ahead of the crack.

according to user-defined traction-separation law, as shown in Figure 5. The traction-separation law determines the strain required for transitioning from initiation to complete failure based on the toughness of the material (characterized as mixed-mode fracture energy, which is the area of the shaded region in Figure 5). The effective separation (δ_m) used in the cohesive failure law is a combination of normal and shear separations, denoted by δ_n and $\delta_{s,t}$, respectively.

$$\delta_m = \sqrt{\delta_n^2 + \delta_s^2 + \delta_t^2} \tag{15}$$

A damage-state variable φ $(0 \le \varphi \le 1)$ is defined based on the separation observed ahead of the crack tip as given in equation (16). δ^o_m is the effective separation at damage initiation and δ^f_m the effective separation at complete failure as shown in Figure 5. The separation at failure is $\delta^f_m - \delta^o_m = 2G_c/T^o_{eff}$, with T^o_{eff} as the effective traction at damage initiation. G_c is the mixed-mode fracture energy as seen in Figure 5. δ^{max}_m is the maximum value of the effective separation δ_m attained during loading history. During damage evolution, the stiffness matrix is reduced based on damage variable φ, and the element is removed when $\varphi = 1$ (fully damaged) at all integration points of the element. The mixed-mode fracture energy, G_c, is assumed to be oxidation-state dependent

$$\varphi = \frac{\delta^f_m\left(\delta^{max}_m - \delta^o_m\right)}{\delta^{max}_m\left(\delta^f_m - \delta^o_m\right)} \tag{16}$$

Oxidation growth and damage evolution in a carbon fiber/polyimide lamina

The oxidation and damage growth during isothermal aging of a carbon fiber (G30) and polyimide (PMR-15) composite were simulated. Oxidation layer growth and damage evolution in both fiber axis direction and transverse to the fiber were simulated for this system. The parameters required for the oxidation model have also been established for this system in prior efforts.[2,3,6]

Mechanical properties

During thermal oxidation of composites, the carbon fiber is stable while the polymer resin undergoes chemical reaction with oxygen and gets oxidized. For G30-500 fiber, the elastic and strength properties are available.[35] The values of elastic modulus of the high-temperature polymer resin (unoxidized and oxidized) were measured by nanoindentation[36,37] and tensile test.[38] The homogenized elastic properties of the G30/PMR-15 unidirectional composite lamina were obtained using homogenization,[39] as shown in Table 1. No experiments are available for the behaviors (strength and fracture toughness) of the oxidized polymer resin. The oxidative axial strength of composite lamina F^t_L was estimated here, which will be determined in later work. It will be shown later, in this research, that this value does not have influence on the results, as both axial and transverse oxidation reach the tensile/transverse failure mode (equation (13)) rather than the tensile/axial failure mode (equation (12)). Table 2 shows the mean strength values of G30/PMR-15 composites, with assumed oxidized composite lamina strength and standard deviation. The assumed standard deviation of strength has been defined as a percentage of the mean. For virgin or unoxidized polymer resin, the critical energy release rate was characterized about $500\,\mathrm{J/m^2}$.[40] However, the oxidized resin and lamina have a much lower fracture toughness and a potential for brittle fracture due to oxidation degradation.[36] A low value ($G_c = 0.5\,\mathrm{J/m^2}$) is assumed for transverse fracture toughness of composite lamina in this study.

The oxygen diffusivity for PMR-15 resin was obtained from literature.[2] Estimates for fiber diffusivity and interphase diffusivity for this system were also determined earlier.[3,6,16] The ratio of oxygen diffusivity of G30/PMR-15 polymer composite to that of the PMR-15 resin was determined to be $D_L/D_m = 7.624$ along the fiber axis and $D_{T,Z}/D_m = 0.335$ transverse to the fiber for both oxidized and unoxidized materials. The values of homogenized properties of D_{un} and D_{ox} in axial and transverse directions for G30/PMR-15 unidirectional composite with 50% fiber volume fraction aging at 288°C are shown in Table 3. The physical and oxidative-shrinkage coefficients are also known for PMR-15 resin at the desired temperature of 288°C.[3,41] The effective oxidation-induced shrinkage coefficients for G30/PMR-15 polymer composite were determined by volume averaging the fiber, unoxidized matrix, and oxidized matrix-shrinkage coefficients using energy principles[22] and are shown in Table 4.

Table 1. Homogenized elastics properties of G30/PMR-15 lamina.

	E_L (GPa)	$E_{T,Z}$ (GPa)	$\nu_{LT,LZ}$	ν_{TZ}	$G_{LT,LZ}$ (GPa)	G_{TZ} (GPa)
Unoxidized	123	7.64	0.313	0.523	3.81	2.5
Oxidized	123	8.79	0.313	0.536	4.59	2.86

Table 2. Homogenized strength properties of G30/PMR-15 lamina.

	F_L^t (MPa)	F_L^c (MPa)	$F_{T,Z}^t$ (MPa)	$F_{T,Z}^c$ (MPa)	$F_{LT,TZ,ZL}^s$ (MPa)	Standard deviation/mean strength (%)
Unoxidized	400	300	40	400	40	1
Oxidized	400	300	20	200	20	10

Table 3. Homogenized oxygen diffusivity of G30/PMR-15 lamina.

	D_m (10^{-3} mm^2/h)	D_L (10^{-3} mm^2/h)	$D_{T,Z}$ (10^{-3} mm^2/h)
Unoxidized	3.216	24.519	1.077
Oxidized	4.680	35.680	1.568

Table 4. Homogenized oxidation-induced shrinkage coefficients of G30/PMR-15 Lamina.

Shrinkage coefficients	α_f	α_m (10^{-6}/h)	α_L (10^{-6}/h)	$\alpha_{T,Z}$ (10^{-6}/h)
Unoxidized	0	−2.5	−0.04797	−1.889
Oxidized	0	−11	−0.2611	−8.295

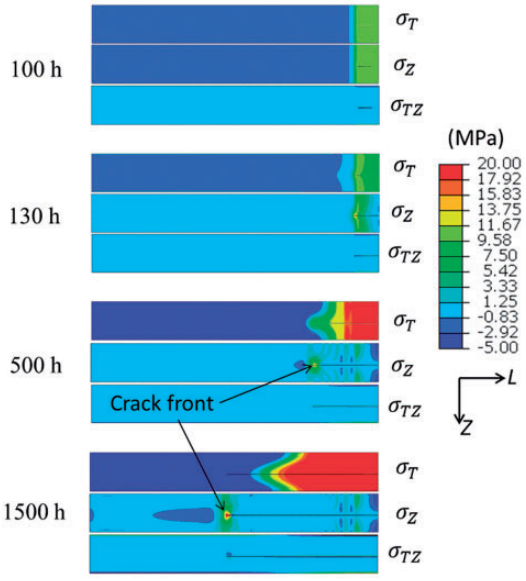

Figure 6. Stress states in a G30/PMR-15 lamina under axial oxidation at selected times during isothermal aging.

Oxidation along the fiber axis

A RVE was chosen from the lamina with a length of 3000 μm (in L-direction), a thickness of 400 μm (in Z-direction), and a width of 100 μm (in T-direction), as shown in Figure 4. The mesh used has 10-μm spacing in axial direction (L-direction). The right face of this RVE was exposed to oxygen, and the oxidation layer grew from right to left through the model along fiber direction (negative L-direction in Figure 4). Oxygen-sorption boundary condition was applied to the right face of this RVE, while other faces were applied periodic boundary condition.

Figure 6 depicts the evolution of three stress components ($\sigma_T, \sigma_Z, \sigma_{TZ}$) simulated at various time intervals during oxidation of the G30/PMR-15 polymer composite aged at 288°C. Figure 7 shows the oxidation and damage states at the same time intervals during aging. The stress contours are shown in the range of +20 MPa to −5 MPa. After 100 h of aging, the oxidized layer thickness reached approximately 290 μm, with oxidation-induced stresses high in the oxidized region ($\sigma_T = 11.1$ MPa and $\sigma_Z = 11.5$ MPa). Transverse tensile failure criterion (equation 13) was reached at specific locations in the model, and the damage began to evolve. At 130 h aging, the oxidized layer thickness reached 392 μm, and the damage variable reached unity indicating that a discrete crack had formed with traction-free crack surfaces (the crack and its length at different aging time is shown in Figure 7). As the new crack surfaces were connected to an oxidizing

boundary, oxygen permeated and adsorbed into the crack surfaces instantaneously. Oxygen diffused ahead of the crack tip creating a newly oxidized zone with lower fracture toughness and accelerated the crack growth. The areas near the vicinity of crack were seen to have substantially larger oxidation zones as opposed to damage-free regions. This result is consistent with the experimental observations.

Figures 8 and 9 show the oxidation and crack growth rates until 2000 h of aging, respectively. These figures also show the correlation between model predictions and experimental observations.[19] The lines indicate simulated results, and discrete symbols represent experimental observations. The discrete crack starts from an initial extent of 70 μm at 130 h and propagates to an extent of 300 μm at 200 h. We define crack extent as the distance from the crack tip to the exposed edge of the RVE, and for straight cracks, the crack extent will be the same as the crack length.

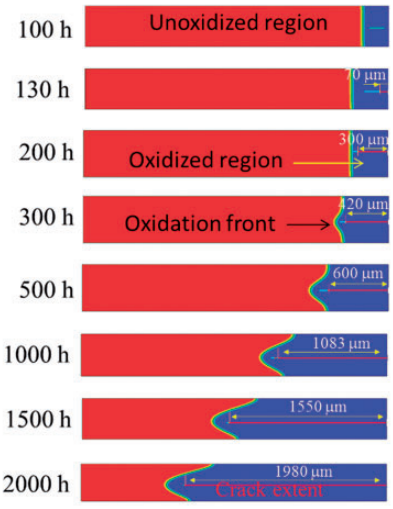

Figure 7. Oxidation layer size and crack extent for G30/PMR-15 lamina under axial oxidation.

Oxidation experiments[19,42] showed that the oxidation layers consistently precede the crack front extent. Oxidative shrinkage causes tensile stresses in the oxidized regions and compression in the unoxidized region. As the transverse tensile strength for the oxidized material is very low (20 MPa assumed) and the compression strength for unoxidized material is much higher (400 MPa) along the fiber, the cracks arrest at the interface between oxidized and unoxidized zones. However, the newly created crack surfaces have high concentration of dissolved oxygen due to adsorption and oxidized zones grow ahead of the crack tips weakening the material within few hours of aging.

The simulated results for both oxidation layer growth and crack front extent correlate well with the experimental data below 1600 h of aging. Above 1600 h, the experimental results do not closely capture the oxidation layer thickness and crack growth. This discrepancy may be attributed to a combination of variability in strength distribution and other heterogeneities, and erosion increased diffusivity due to cracking. These effects are predominant after thousands of hours aging. Figures 8 and 9 show the variability in the average oxidation layer length and crack extent measured in the experiments, respectively.[19] The data shows that

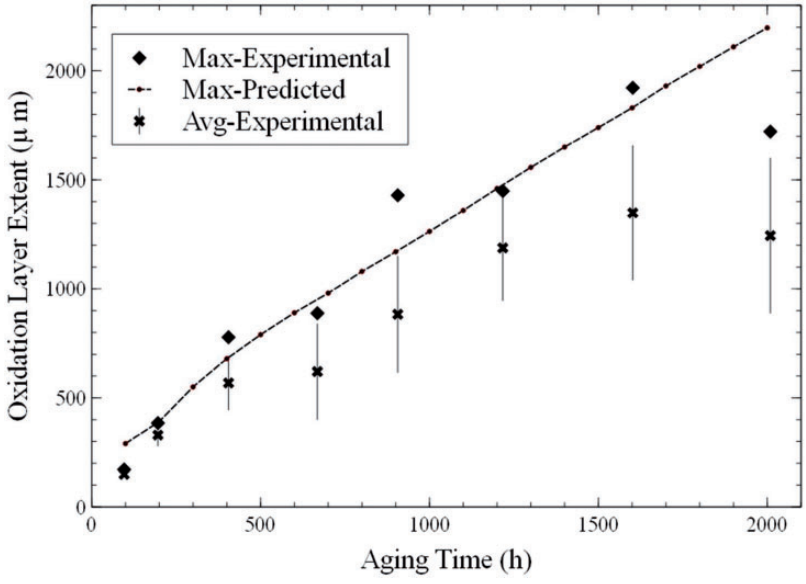

Figure 8. Correlation of predictions and experimental observations for oxidation growth under axial oxidation.

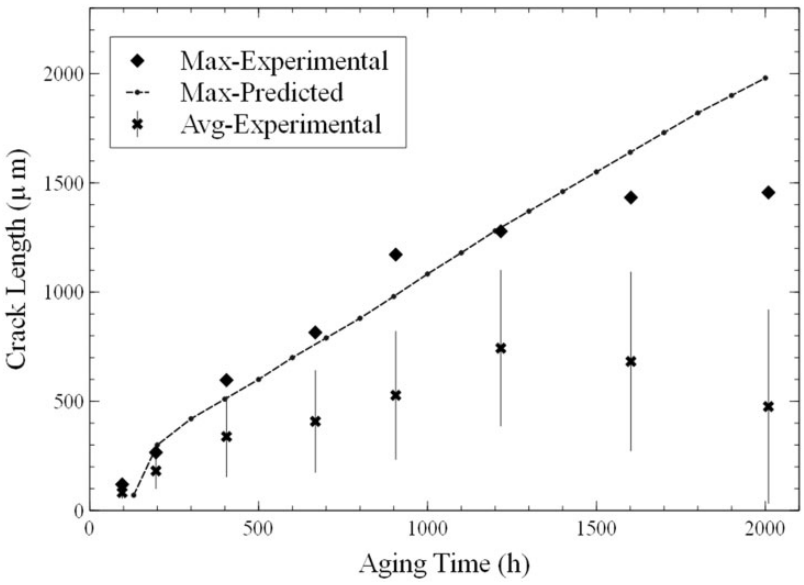

Figure 9. Correlation of predictions and experimental observations for crack growth under axial oxidation.

there is considerable variability in the observation as indicated by the error bars representing the standard deviation ($\pm\sigma$).

Oxidation transverse to the fiber

The RVE for oxidation simulation in the transverse direction, as shown in Figure 4, had a length of 1000 μm (in Z-direction), width 400 μm (in T-direction), and thickness 100 μm (in L-direction). The mesh used has 6.67-μm spacing in Z-direction. The top face of this RVE was exposed to oxygen, and the oxidation layer grew from top to bottom through the model along Z-direction. Oxygen saturation boundary condition was applied to the top face of this RVE, while other faces were applied periodic boundary condition. The experimental data for oxidation progression and crack growth with time was also obtained from Tandon et al.[19]

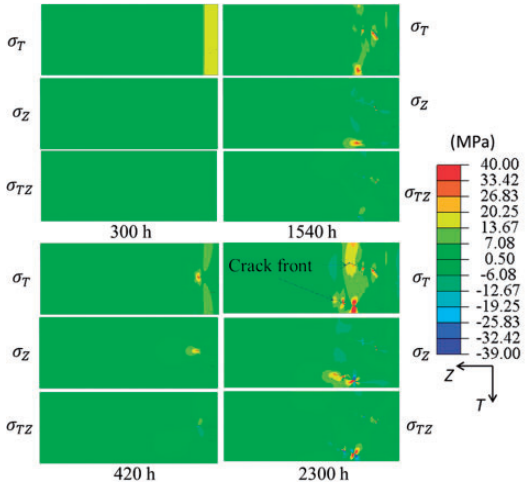

Figure 10. Evolution of stress and damage in a G30/PMR-15 lamina under transverse oxidation.

Figure 10 shows three stress components in the lamina at selected time intervals after several thousand hours of simulated isothermal aging at 288°C. One point to note is that the RVE has been rotated, and so the oxidation also grows from right to left through the model (the T- and Z-directions are shown in Figure 10). Figure 11 shows the evolution of the oxidation and damage states during aging under the same conditions. After 300 h of aging, the oxidized layer thickness reached 98.67 μm, with the stresses high in transverse directions ($\sigma_T = 15.8$ MPa and $\sigma_Z = 3.7$ MPa). Damage initiation criterion (equation 13) had been reached at several locations in the oxidized regions. Damage initiated at three locations in the model. Imposing a different model for the spatial variability of the strength can alter the location and number of cracks. The location and number may also change based on the random sampling from the strength distribution. Multiple simulations (Monte-Carlo analyses) were not performed to study the influence of the randomness on the crack location and number in a statistically significant fashion. However, limited number of runs was performed to check that cracks initiated consistently at the same time increment in the analysis.

The first crack fully developed at an aging time of 420 h, and the second crack developed more slowly at 1540 h due to parallel nature of the multiple cracks and

the unloading in the vicinity of the first crack. Figure 11 depicts the crack extent for both the cracks at several selected time intervals. The figure also shows the oxidation layer growth. Unlike the straight self-similar propagation in the axial direction, the transverse cracks are seen to meander within the oxidized zone.[19] Figure 12 shows the oxidation in front of both the first crack (oxidation 1) and the second crack (oxidation 2). The experimental observations for maximum oxidation front are also plotted as symbols in this figure. The data shows that the predicted oxidation layer sizes correlate well for approximately 1700 h, and the simulation under predicts the oxidation layer size at 3000 h. The discrepancy can be attributed to several issues. There is a considerable uncertainty in the strength and toughness values within the oxidized materials due to porosity, erosion, and loss of load transfer abilities due to the degradation of fiber-matrix interface. Furthermore, heterogeneity exists in the experimental observations, and the maximum crack length varies considerably from specimen to specimen. In any case, the simulations have not captured the behavior of the oxidation layer growth after 1700 h. Figure 13 shows the crack growth data predicted by the simulations and the maximum crack length observed experimentally. Figure 14 shows both the maximum oxidation layer thickness and crack extent data obtained from simulations and a comparison with that determined in experiments. The data shows that the predicted oxidation layer thickness correlates well with the experimental observations below 1700 h, and crack propagation correlates well with the experimental below 2100 h.

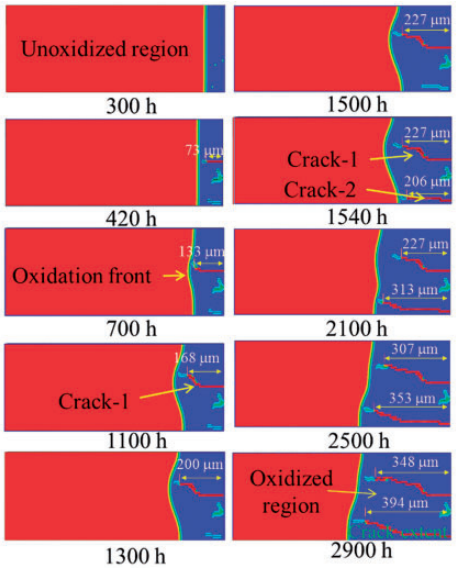

Figure 11. Oxidation growth and crack sizes for a G30/PMR-15 lamina under transverse oxidation.

The damage growth in the transverse direction is substantially lower than the axial direction due to two reasons. First, the fracture toughness is substantially higher in the transverse direction due to the reinforcing fibers. Second, the crack kinks to stay within the oxidized regions due to lower toughness and does not penetrate the unoxidized regions. For example, the crack extent in axial direction at 1500 h is seen to be about 1550μm while that in the transverse direction is about 227μm.

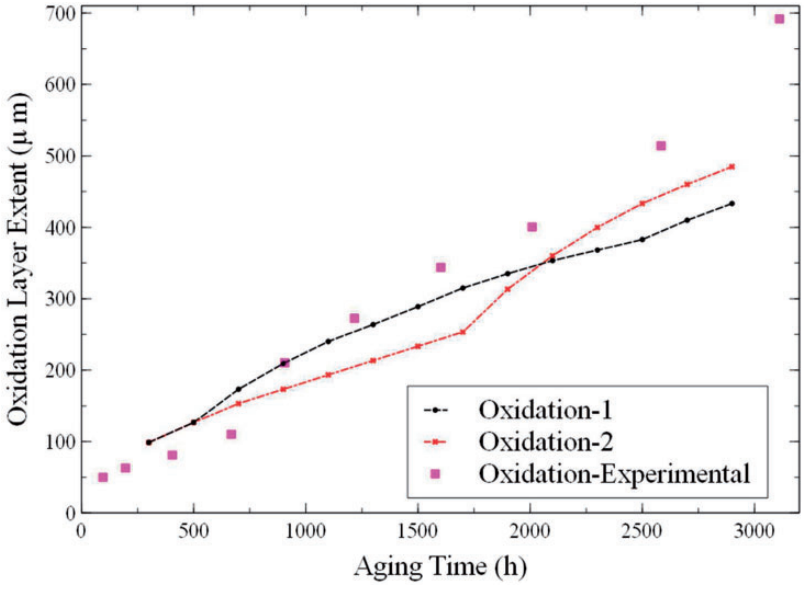

Figure 12. Correlation of simulated and experimental oxidation layer size measurements under transverse oxidation.

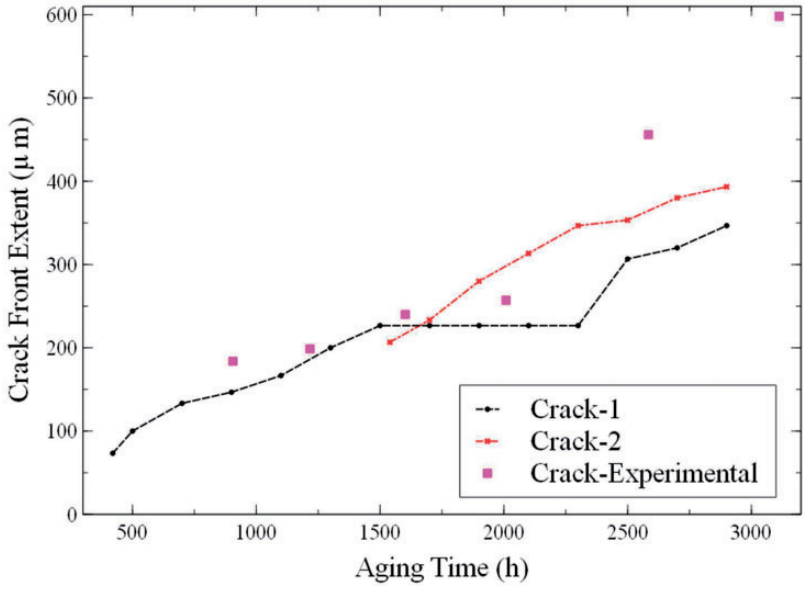

Figure 13. Correlation of crack extent predictions and experimental observations under transverse oxidation.

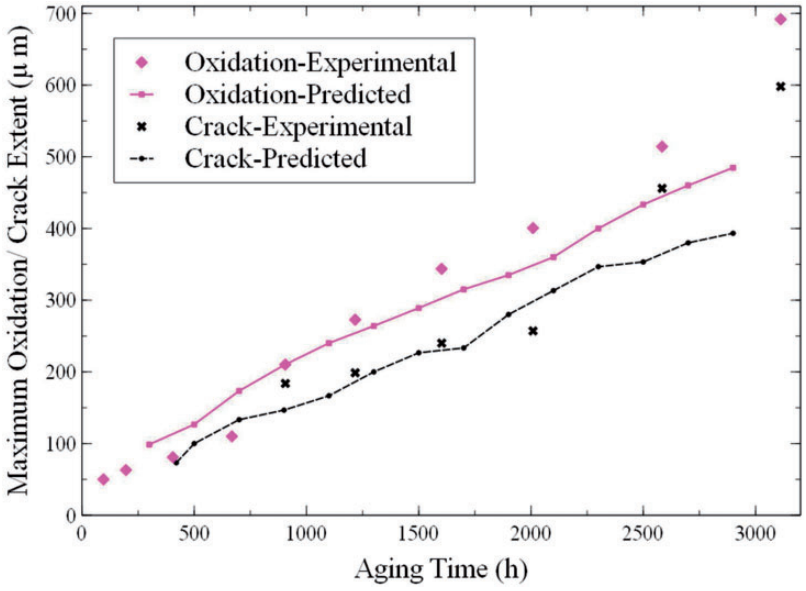

Figure 14. Correlation of oxidation layer sizes and crack extent for oxidation under transverse oxidation.

Concluding remarks

Thermal oxidation growth and damage evolution are highly coupled. Oxidation causes morphological changes and weaker oxidized materials and mismatch strains due to chemical changes. Damage evolving in the oxidized regions exacerbates the thermo-oxidation by providing additional surfaces for oxygen sorption and increasing the dissolved oxygen concentration available for the oxidation reaction. Prediction of long-term durability requires consideration of both oxidative changes and damage evolution.

A comprehensive oxidation-mechanics-damage model has been proposed in this paper. This methodology considers the coupling of oxidation growth and damage evolution. Detailed damage evolution characteristics and oxidation patterns are obtained during isothermal aging of a composite lamina. Oxidation growth and crack propagation for a carbon fiber (G30) and polyimide matrix (PMR-15) composite have been simulated over thousands of hours of use under isothermal conditions. The obtained oxidation growth and damage evolution correlate well with experimental observations.

In a composite lamina, the high-oxygen diffusivity direction (along the fiber axis) also has a low-transverse strength. Therefore, larger regions of degradation are evident when the edges of the lamina are exposed to oxygen. As the surface that is typically exposed to oxidation in a composite structure is the top skin layer, which is subjected only to transverse oxidation, the accelerated degradation from axial crack growth, in practice, may not be significant. However, edges created by holes, notches, and other features in the composite may have to be specially designed or protected with coatings to prevent the accelerated degradation.

Acknowledgements

The authors gratefully acknowledge partial funding from the US Air Force Office of Scientific Research (AFOSR) through the contract no. FA9550-09-1-0439. We thank Dr J Harrison, Program Manager, Low Density Materials Program, for the support.

Conflict of interest

None declared.

Funding

This research received no specific grant from any funding agency in the public, commercial, or not-for-profit sectors.

References

1. Bowles KJ and Nowak G. Thermo-oxidative stability studies of Celion 6000/PMR-15 unidirectional composites, PMR-15, and Celion 6000 fiber. *J Compos Mater* 1988; 22: 966–985.
2. Pochiraju KV and Tandon GP. Modeling thermo-oxidative layer growth in high-temperature resins. *J Eng Mater Technol-Trans ASME* 2006; 128: 107–116.
3. Pochiraju KV, Tandon GP and Schoeppner GA. Evolution of stress and deformations in high-temperature polymer matrix composites during thermo-oxidative aging. *Mech Time-Depend Mater* 2008; 12: 45–68.
4. Tandon GP. Characterization of thermo-oxidation in laminated and textile composites. In: Pochiraju KV, Tandon GP and Schoeppner GA (eds) *Long-term durability of polymeric matrix composites*. USA: Springer, 2012, pp.345–382.
5. Weitsman Y. Stress assisted diffusion in elastic and viscoelastic materials. *J Mech Phys Solids* 1987; 35: 73–94.
6. Pochiraju K and Tandon GP. Interaction of oxidation and damage in high temperature polymeric matrix composites. *Composites Part A* 2009; 40: 1931–1940.
7. Colin X, Marais C and Verdu J. A new method for predicting the thermal oxidation of thermoset matrices: application to an amine crosslinked epoxy. *Polym Test* 2001; 20: 795–803.
8. Skontorp A, Wong M-S and Wang S-S. High temperature anisotropic thermal oxidation of carbon fiber-reinforced polyimide composites: theory and experiment. In: *Proceedings of the 10th international conference on composite materials*, Vancouver, Canada, 1995, pp.382–385.
9. Audouin L, Langlois V, Verdu J, et al. Role of oxygen diffusion in polymer ageing: kinetic and mechanical aspects. *J Mater Sci* 1994; 29: 569–583.
10. McManus HL, Foch BJ and Cunningham RA. Mechanism-based modeling of long-term degradation. In: Reifsnider KL, Dillard DA and Cardon AH (eds) *Proceedings of the third international conference on progress in durability analysis of composite systems*, DTIC document, Blacksburg, Virginia, 1997, pp.63–70.
11. Johnson WS, Masters JE, O'Brien TK, et al. Modeling damage in a plain weave fabric-reinforced composite material. *J Compos Technol Res* 1993; 15(2): 136–142.
12. Fang G, Liang J and Wang B. Progressive damage and nonlinear analysis of 3D four-directional braided composites under unidirectional tension. *Compos Struct* 2009; 89: 126–133.
13. Bouchard PO, Bay F, Chastel Y, et al. Crack propagation modelling using an advanced remeshing technique. *Comput Methods Appl Mech Eng* 2000; 189: 723–742.
14. Belytschko T and Black T. Elastic crack growth in finite elements with minimal remeshing. *Int J Numer Methods Eng* 1999; 45: 601–620.
15. Melenk JM and Babuška I. The partition of unity finite element method: basic theory and applications. *Comput Methods Appl Mech Eng* 1996; 139: 289–314.
16. Yu Y-T and Pochiraju K. Modeling long-term degradation due to moisture and oxygen in polymeric matrix composites. *Mater Sci Eng A* 2008; 498: 162–165.
17. Tandon GP, Pochiraju KV and Schoeppner GA. Modeling of oxidative development in PMR-15 resin. *Polym Degrad Stab* 2006; 91: 1861–1869.
18. Tandon GP, Briggs J and Schoeppner GA. Thermo-oxidative degradation of carbon fibers for high-temperature polymer matrix composites. In: *Proceedings of American society for composites, 21st technical conference*, Dearborn, MI, 2006, pp.1296–1311.
19. Tandon G, Ragland W and Schoeppner G. Using optical microscopy to monitor anisotropic oxidation growth in high-temperature polymer matrix composites. *J Compos Mater* 2009; 43: 583–603.
20. Abdeljaoued K. *Study of matrix thermal oxidation in carbon fibers-PMR-15 composites*. PhD Thesis, ENSAM Paris, 1999.
21. Schoeppner GA, Tandon GP and Ripberger ER. Anisotropic oxidation and weight loss in PMR-15 composites. *Composites Part A* 2007; 38: 890–904.
22. Schapery RA. Thermal expansion coefficients of composite materials based on energy principles. *J Compos Mater* 1968; 2: 380–404.
23. Motamedi D and Milani AS. 3D nonlinear XFEM simulation of delamination in unidirectional composite laminates: a sensitivity analysis of modeling parameters. *Open Journal of Composite Materials (OJCM)* 2013; 3: 113–127.

24. Harrison RP and Bader MG. Damage development in CFRP laminates under monotonic and cyclic stressing. *Fibre Sci Technol* 1983; 18: 163–180.
25. Nairn JA. Matrix microcracking in composites. Chapter 13. *Polym Matrix Compos* 2000; 1–34.
26. Andersons J, Spārniņš E and Joffe R. Prediction of crack onset strain in composite laminates at mixed mode cracking. *IOP Conf Ser Mater Sci Eng* 2009; 5: 012–018.
27. Wang AS. Fracture analysis of matrix cracking in laminated composites, No. NADC-85118-60, Drexel University, 1985.
28. Hashin Z and Rotem A. A fatigue failure criterion for fiber reinforced materials. *J Compos Mater* 1973; 7: 448–464.
29. Davila CG, Camanho PP and Rose CA. Failure criteria for FRP laminates. *J Compos Mater* 2005; 39: 323–345.
30. Wu W-F, Cheng H-C and Kang C-K. Random field formulation of composite laminates. *Compos Struct* 2000; 49: 87–93.
31. Barber A, Kaplanashiri I, Cohen S, et al. Stochastic strength of nanotubes: an appraisal of available data. *Compos Sci Technol* 2005; 65: 2380–2384.
32. Goda K, Okabe T and Takeda N. A strength reliability model of unidirectional fiber-reinforced ceramic matrix composites by Markov process. *Adv Compos Mater* 2006; 15: 263–285.
33. McCartney LN. Model to predict effects of triaxial loading on ply cracking in general symmetric laminates. *Compos Sci Technol* 2000; 60: 2255–2279.
34. Liang J and Pochiraju K. A probabilistic strength distribution model in predicting damage evolution due to thermo-oxidation of polymeric matrix composites. In: *Proceedings of ASME 2013 international mechanical engineering congress and exposition*, San Diego, CA, 2000, pp.1–9.
35. McMahon PE. Carbon fiber, Evolving technology. In: LEE SM (ed.) *Handbook of composite reinforcements*. Palo Alto, CA: John Wiley & Sons, 1992, pp.74–76.
36. Lu YC, Tandon GP, Jones DC, et al. Elastic and viscoelastic characterization of thermally-oxidized polymer resin using nanoindentation. *Mech Time-Depend Mater* 2009; 13: 245–260.
37. Minervino M, Gigliotti M, Lafarie-Frenot MC, et al. The effect of thermo-oxidation on the mechanical behaviour of polymer epoxy materials. *Polym Test* 2013; 32: 1020–1028.
38. Ryther CEC and Ruggles-Wrenn MB. The rate (time)-dependent mechanical behavior of the PMR-15 thermoset polymer at temperatures in the 274–316°C range: experiments and modeling. *J Pressure Vessel Technol* 2012; 134: 1–8.
39. Agarwal BD, Broutman LJ and Chandrashekhara K. *Analysis and performance of fiber composites*. New Jersey: John Wiley & Sons, Inc, 2006.
40. Gibbs HH. High temperature resins. In: Peters ST (ed.) *Handbook of composites*. Cleveland, Ohio: Chapman & Hall, 1998, pp.75–98.
41. Luo H, Lu G, Roy S, et al. Characterization of the viscoelastic behavior of bismaleimide resin before and after exposure to high temperatures. *Mech Time-Depend Mater* 2013; 17: 369–399.
42. Tandon GP. Characterization of thermo-oxidation in laminated and textile composites. In: *Long-term durability of polymeric matrix composites*. USA: Springer, 2012, pp.345–382.